Received June 26, 2021, accepted July 20, 2021, date of publication July 26, 2021, date of current version August 2, 2021.

Digital Object Identifier 10.1109/ACCESS.2021.3099305

An Assembly Quality Inspection System for Bone Conduction Implant Transducers

DONG HO SHIN[1] AND HUI-SUP CHO[2]

[1]Institute of Biomedical Engineering Research, Kyungpook National University, Daegu 41944, South Korea
[2]Division of Electronics and Information System, Daegu Gyeongbuk Institute of Science and Technology (DGIST), Daegu 42988, South Korea

Corresponding author: Hui-Sup Cho (mozart73@dgist.ac.kr)

This work was supported in part by the National Research Foundation of Korea (NRF) Grant through by the Korean Government (MSIP) under Grant NRF-2019R1C1C1006176, and in part by Daegu Gyeongbuk Institute of Science and Technology (DGIST) Research and Development Program of the Ministry of Science and ICT, South Korea.

ABSTRACT We designed and implemented a two-axis measurement system to inspect the assembly quality condition of a bone conduction implant (BCI) transducer. The system consists of a laser Doppler vibrometer (LDV), XY manual stage, and two digital scale calipers capable of displaying a position coordinate system. To measure the vibration of the cantilever constituting the transducer vibrational membrane, an XY coordinate system was obtained using FEA software. Based on the derived XY coordinate system, the cantilever vibration displacement of the vibrational membrane was measured for each coordinate using the LDV at 0.5, 0.9, and 2 kHz. To visualize the measured area, we developed a Matlab-based application and then visualized the motion of the cantilever. The alignment and misalignment models of the vibrational membrane and permanent magnet were designed using finite element analysis (FEA) software, and the measured cantilever motions of the vibrational membrane were then compared. Finally, to numerically compare the vibration magnitude of the cantilever, the standard deviation was calculated based on the displacement of each edge of the cantilever. The fabricated BCI transducer had a higher standard deviation (3.5 times at 0.5 kHz, 2.3 times at 0.9 kHz) than the ideally aligned FEA model, but the standard deviation was about eight times lower (at 0.5 and 0.9 kHz) than that of the misaligned case. The results of the numerical comparison indicated that the manufactured BCI transducer was very well assembled.

INDEX TERMS Bone conduction implant transducer, vibrational membrane with cantilever structure, assembly quality inspection system, finite element analysis.

I. INTRODUCTION

People with hearing impairments commonly use hearing aid devices to improve their hearing, including air conduction hearing aids and middle-ear implants (MEI) [1]–[4]. These hearing aids provide assistance according to the degree of hearing loss by using sound signals (sound pressure) or vibrational signals corresponding to sound [5]–[8]. Air conduction hearing aids are the most widely available hearing aids on the market, but are not suitable for people with severe hearing impairments due to limited maximum output. In addition, there are problems associated with occlusion effects of the ear canal and acoustic feedback [8]–[10]. To compensate for the limitations of these air conduction hearing aids, MEI that transmit mechanical vibrational signals instead of acoustic signals have been developed [11]–[16]. In typical MEI, a small transducer is attached to the auditory ossicles to transmit vibrational signals directly to the cochlea. As MEI generate vibrational rather than sound signals, they are unaffected by the noisy feedback associated with air conduction hearing aids, and because the auditory path is used without modification, it can deliver natural sounds. In addition, even if a transducer is implanted in the auditory ossicles, it does not significantly affect residual hearing. However, MEI are not preferred by many patients with hearing loss because they require complicated invasive surgery, unlike noninvasive air conduction hearing aids. In addition, they cannot be applied in cases of hearing impairment where sound is not effectively transmitted to the cochlea due to damage to the auditory ossicles of the ear [17]–[20].

Recently, bone conduction implants (BCI) have been developed that can be applied in people with hearing impairment who cannot use conventional hearing aids [21]–[24]. BCI are attracting increasing attention as a rehabilitation

The associate editor coordinating the review of this manuscript and approving it for publication was Michail Kiziroglou.

option for patients with hearing loss, and are currently undergoing clinical trials [25], [26]. In addition, BCI have the advantage that implantation requires only minimally invasive surgery with no risk of damaging residual hearing [27], [28]. BCI devices are implanted behind the ear in the mastoid area and transmit vibrational signals to the cochlea through the skull using a transducer like MEI [29]. However, while the vibrations propagate through the bone and into the cochlea, the vibrational signals generated by the transducer are subject to significant loss. Therefore, it was necessary to develop a new structured transducer capable of generating high vibrations.

To increase the output of the bone conduction transducer, Shin *et al.* [30] proposed a prototype electromagnetic transducer with a dual coil structure. The mechanical resonance frequency of the transducer was adjusted using a vibrational membrane with a multiple-cantilever structure. Lee *et al.* [31] improved the miniaturization and frequency characteristics so that the prototype transducer could be used as a BCI. The output characteristics of the improved transducer were evaluated by functional near-infrared spectroscopy (fNIRS). Shin *et al.* and Lee *et al.* focused on improving vibration output when developing transducers for BCI. However, for hearing aid transducers, not only the output magnitude but also the distortion characteristics must be taken into consideration. This is because a transducer with high distortion characteristics has a high risk of unwanted sound generation when converting an acoustic signal into a vibrational one. Therefore, reducing distortion of the transducer is as important as increasing the output magnitude.

The improved transducer reported by Lee *et al.* [31] has a permanent magnet coupled to the center of a vibrational membrane composed of three cantilevers. When a current flows through the coil, the magnet vibrates due to the interaction between the coil and magnet. In addition, as the vibrational membrane and magnet are connected, the cantilever also vibrates. As the frequency characteristics of the vibrational membrane is measured using a laser Doppler vibrometer (LDV) at only one central point, it is difficult to check the alignment of the vibrational membrane and magnet. If the magnet is ideally aligned with the central axis of the vibrational membrane, the vibration shape of each cantilever will be almost the same. However, if the magnet connected to the vibrational membrane vibrates up and down in a state that deviates from the central axis due to misalignment, each cantilever has a different vibration shape due to the rolling phenomenon. Due to this phenomenon, distortion of the transducer may increase, so an inspection system is required to confirm the assembly condition of the transducer.

Here, we implemented a two-axis manual measurement system to analyze the assembly state of a BCI transducer using single-point LDV. The measurement system consists of an XY stage and two digital scale calipers capable of expressing a position coordinate system. To minimize the distortion of the cantilever, the number of cantilevers in the transducer structure of Lee *et al.* [31] was changed from three to four, with the remaining components manufactured in the same way. In addition, the XY coordinate system of the cantilever shape was derived using finite element analysis (FEA) software. Based on the derived coordinate system, vibrational displacement of the assembled transducer vibrational membrane was measured using LDV. To represent the areas where vibrational displacement was measured as polygons, a Matlab (MathWorks Inc., Natick, MA, USA)-based application was developed and the movement of the cantilever-structured membrane was visualized. Finally, the assembly condition of the transducer was confirmed by comparing the measured displacement of each cantilever.

II. METHODS

A. IMPLEMENTATION OF THE BCI TRANSDUCER

The BCI consists of an external device with a microphone and signal processing part, and an internal device with a transducer and demodulator. The external sound signal collected through the microphone is processed, transmitted wirelessly to the internal device, and then converted into a vibrational signal in the transducer. The vibrational signal generated by the transducer propagates along the skull to the cochlea. As sound is transmitted to the hearing-impaired person through this mechanism, it is important that the transducer, the final output device of BCI, converts sound signals into vibrational signals without distortion. As the electromagnetic-type transducer has many internal components, distortion may occur due to misalignment during assembly. In addition, it is difficult to check for misalignment after the BCI transducer is completely assembled. Therefore, a system that can check for misalignment between transducer components before the transducer is fully assembled is needed.

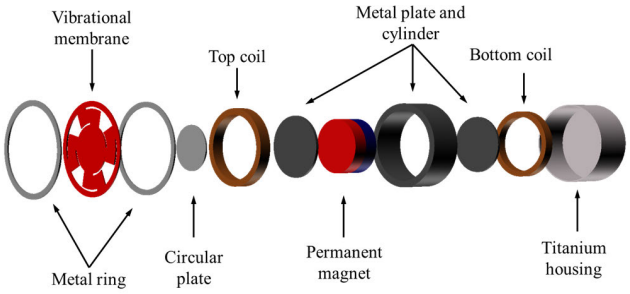

FIGURE 1. Components of the experimental BCI transducer.

To manufacture a transducer for use in the experiment, the specifications of the transducer made by Lee *et al.* [31] were used without modification. Here, unlike the previous transducers, the number of cantilevers was increased from three to four because when a vibrational membrane has the same resonance frequency, a vibrational membrane composed of three cantilevers is longer than when there are four cantilevers. Therefore, the stiffness decreases as the number of cantilevers increases. When the permanent magnet deviates from its alignment and approaches the metal cylinder, a rolling

phenomenon occurs due to the attractive force between the permanent magnet and the metal cylinder during vibration. As a result, when the transducer has three cantilevers rather than four, distortion is more likely to occur. The number of cantilevers was increased from three to four to minimize distortion by reducing the length of the cantilevers. The BCI transducer consists of a metal ring, circular plate, vibrational membrane with four cantilevers, metal plate and cylinder, permanent magnet, top (forward) and bottom (reverse) coils wound in opposite directions, and titanium housing (Fig. 1). The transducer used in the experiment was 15 mm in diameter and 8 mm in height. The titanium cover of the transducer with screw holes was not considered in this study because it was not necessary for the experiment.

In most cases, the resonance frequency of a BCI transducer is between 0.7 and 1 kHz [32]. Therefore, mechanical vibration analysis was required to match the resonance frequency of the 4-cantilever transducer to that of the previous transducer (mechanical resonance = 0.9 kHz). The resonance frequency of the transducer is determined by the stiffness of, and mass applied to, the vibrational membrane. The stiffness of the vibrational membrane can be controlled by modifying several parameters, such as the width, thickness angle, and number of cantilevers. To simplify the FEA procedure, the thickness and width of the cantilever were both fixed at 0.2 mm, and mechanical vibration analysis was performed using FEA software (Multiphysics 5.5; COMSOL Inc., Stockholm, Sweden) only for the angle of the cantilever. Fig. 2(a) shows the shape of the vibrational membrane with four cantilevers, each of which was constructed based on origin symmetry. In mechanical vibration analysis, only the vibrational membrane and mass components (permanent magnet, metal plate, and circular plate), which are the factors determining the resonance frequency, are expressed. The mesh model is shown in Fig. 2(b). All elements of the mesh model were constructed in a 3D environment, and the total force (486.4 mN) and total mass (2.77 g) applied to the vibrational membrane were set using a solid mechanics routine. Here, the total force applied to the vibrational membrane is the value obtained based on the electromagnetic analysis results of Lee *et al.* [31]. The rim of the vibrational membrane, which does not affect the vibration, was fixed (“fixed constraint)”, and displacement of the permanent magnet, two metal plates, and cantilevers was set to “free/free.” The analysis model applied a “free tetrahedral” mesh, and consisted of 130,939 domain elements, 32,594 boundary elements, and 3,716 edge elements (maximum element size, 0.483 mm; minimum element size, 0.0207 mm; maximum element growth rate, 1.35; curvature factor, 0.3; narrow-region resolution, 0.85). The material properties of the vibrational membrane were as follows: density, 8,000 kg/m^3; Poisson’s ratio, 0.3; Young’s modulus, 193E9 N/m^2. Mechanical vibration analysis was performed repeatedly while changing the angle of the cantilever from 28° to 48° in increments of 4°. Fig. 2(c) and (d) show the von Mises stress distribution (representing the maximum energy density) obtained through static analysis, and the frequency response characteristic obtained by dynamic analysis, respectively. The maximum stress of the cantilever based on the

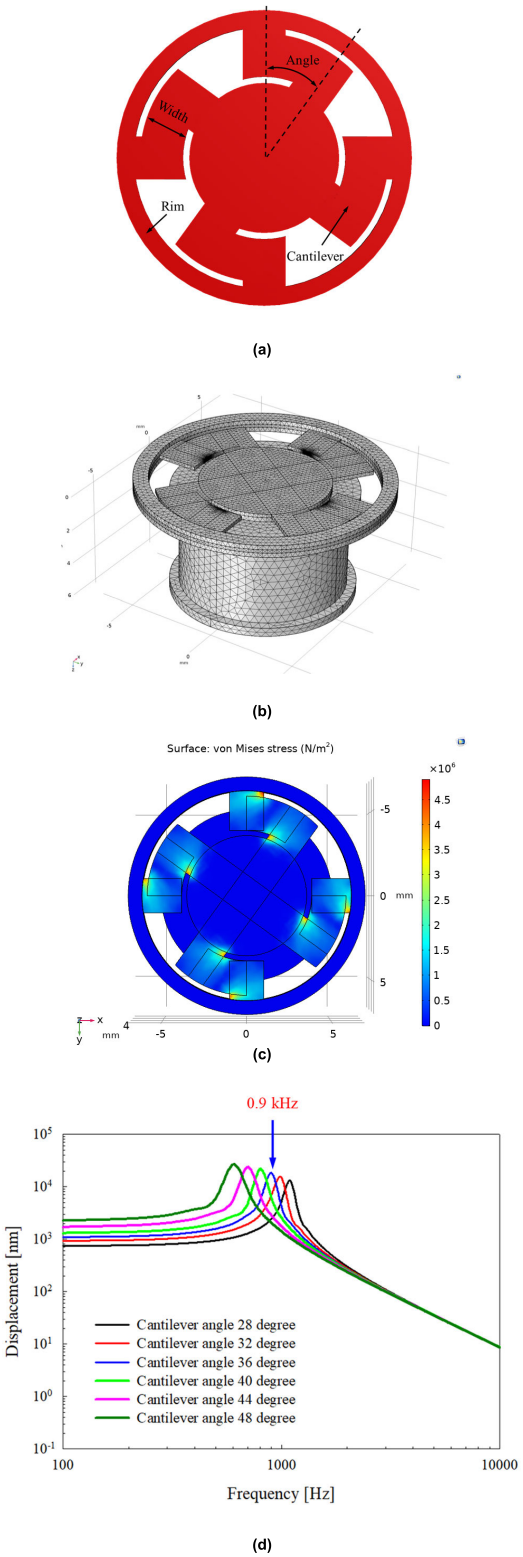

FIGURE 2. (a) Shape of the vibrational membrane with four cantilevers. (b) Mesh model for mechanical vibration analysis. (c) The von Mises stress distribution producing the maximum distortion energy density of the vibrational membrane. (d) Vibrational characteristics according to cantilever angle.

static analysis was 5.38e6 N/m^2. According to the results of dynamic analysis, with a cantilever angle of 36°, the resonance frequency of the vibrational membrane is 0.9 kHz.

Based on the results of the analysis, BCI transducer components were manufactured by a CNC process and wire electrical discharge machining works. The specifications of the BCI components were as follows: vibrational membrane with a 4-cantilever (diameter, 13.8 mm; angle, 36°; thickness, 0.2 mm; SUS316L), circular plate (diameter, 7 mm; thickness, 0.2 mm; SUS316L), metal ring (outer diameter, 13.8 mm; inner diameter, 12.2 mm; thickness, 0.25 mm), metal cylinder (outer diameter, 13.8 mm; inner diameter, 12.2 mm; height, 6 mm; Mu-metal), metal plate (diameter, 10 mm; height, 0.5 mm; Mu-metal), titanium housing (outer diameter, 15 mm; inner diameter, 13.8 mm; height, 7.5 mm; Ti-6Al-4V), coil (outer diameter, 12.2 mm; inner diameter, 10.2 mm; height, 2 mm; 180 Ω), and permanent magnet (diameter, 9 mm; height, 5 mm; NdFeB, grade N38AH). Each fabricated element was precisely assembled on a probe station equipped with a microscope and precision jig. Fig. 3(a) shows the fabricated transducer components and transducers, assembled without the cover used for testing. To check the frequency characteristics of the assembled transducers, a bench test was performed using an LDV (OFV-5000 vibrometer controller, OFV-534 interferometer sensor head; Polytec GmbH, Waldbronn, Germany) and a data acquisition device (fast Fourier transform length, 4,096; sampling rate, 96 kHz; average, 10; data acquisition systems, NI PXIe-1071, NI PXIe-8840, and NI PXI-4461; National Instruments Co., Austin, TX, USA). The sinusoidal voltage applied to drive the transducer (2.88 V_p) and measurement method were the same as described by Lee *et al.* [31], and the results are shown in Fig. 3(b). The assembled transducer had a resonant frequency at 0.9 kHz, and the vibrational characteristics (black line) were similar to the FEA results (blue line).

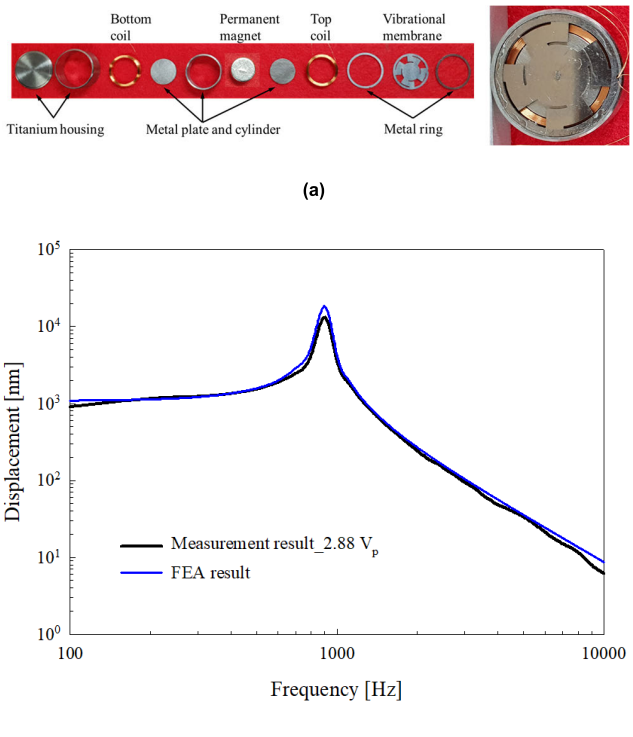

FIGURE 3. (a) Fabricated BCI transducer. (b) Comparison of vibrational characteristics between the measurement and FEA results.

B. XY COORDINATE SYSTEM OF THE CANTILEVER

Distortion of the transducer is likely to be caused by the vibrational membrane, which is the vibrating part among the internal components. In an electromagnetic-type BCI transducer, the coil is firmly fixed to the titanium housing, and the magnet connected to the vibrational membrane vibrates in the vertical direction due to the electromagnetic interaction when current flows through the coil. However, if the center of the magnet and center of the vibrational membrane deviate slightly, the magnet will vibrate while shaking left and right instead of vertically. As a result, the four cantilevers will have different vibrational characteristics.

In the previous measurement method, only one center point of the vibrational membrane was measured using a single-point LDV, to check the vibration magnitude and frequency tendency of the transducer. Therefore, it was difficult to check the alignment between the magnet and vibrational membrane with the previous method. To check the alignment between the magnet and vibrational membrane, the vibrational characteristics of each cantilever must be measured and compared. To compare the vibrational characteristics of each cantilever while moving, it is necessary to measure at the same position, so an XY coordinate system for the shape of the cantilever is required. Using a 3D vibrational membrane model designed in COMSOL software, a total of 121 points were marked at 0.3-mm intervals along the centerline of each cantilever based on the center point (0,0) of the vibrational membrane, as shown in Fig. 4. Then, the XY coordinate values of each point were obtained using the ''Measure'' command.

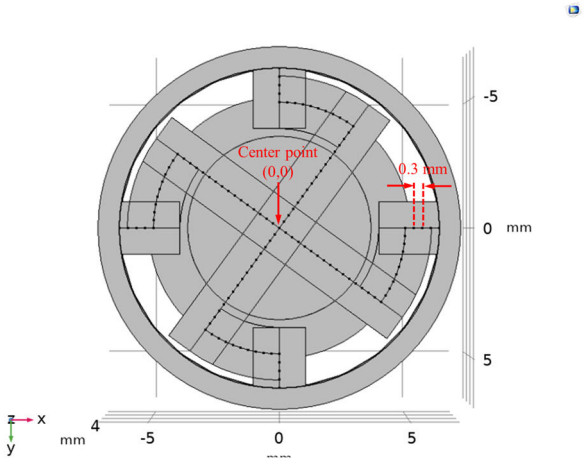

FIGURE 4. The 3D vibrational membrane model used to derive the XY coordinate values of the cantilever.

C. TRANSDUCER ASSEMBLY QUALITY MEASUREMENT SYSTEM

A two-axis manual measurement system for transducer assembly quality inspection (i.e., to check the alignment of the vibrational membrane and magnet) was fabricated. The system consisted of an XY manual stage (XYFG40; MISUMI Group Inc., Tokyo, Japan) that can be fine-tuned and two vertical linear digital scale calipers that display positional information. As shown in Fig. 5, the two digital scale calipers were connected to the X- and Y-axes of the manual stage, so that the moving distance of the manual stage was displayed on the LCD screen. To match the center of the stage of the upper plate with that of the vibrational membrane, an aluminum plate with a groove of the same size as the diameter of the transducer was connected.

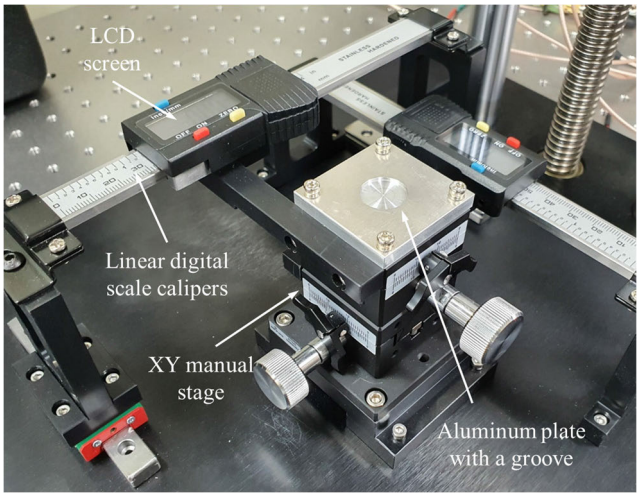

FIGURE 5. Fabricated two-axis manual measurement system to check the alignment of the transducer components.

III. RESULTS

A. FEA ALIGNMENT ANALYSIS

Mechanical vibration analysis was performed to assess the vibrational characteristics according to the alignment of the vibrational membrane and magnet. To misalign the coupling state of the vibrational membrane and magnet in Fig. 2(b), the magnet was moved 0.2 mm from the central axis along the Y-axis, as shown in Fig. 6(a). Then, the analysis was performed in the same way as in the mechanical vibration analysis shown in Fig. 2. The frequency response characteristics at the center point of the vibrational membrane are shown in Fig. 6(b) according to the alignment of the vibrational membrane and magnet. Comparison of the output of the misaligned case (red line) with that of the aligned case (blue line) showed that the frequency characteristics differed within a specific frequency band.

This result corresponds to the frequency characteristic caused by distortion. However, to accurately determine whether the output characteristic is due to distortion of the vibrational membrane, it is necessary to analyze all points according to the coordinate system of the cantilever.

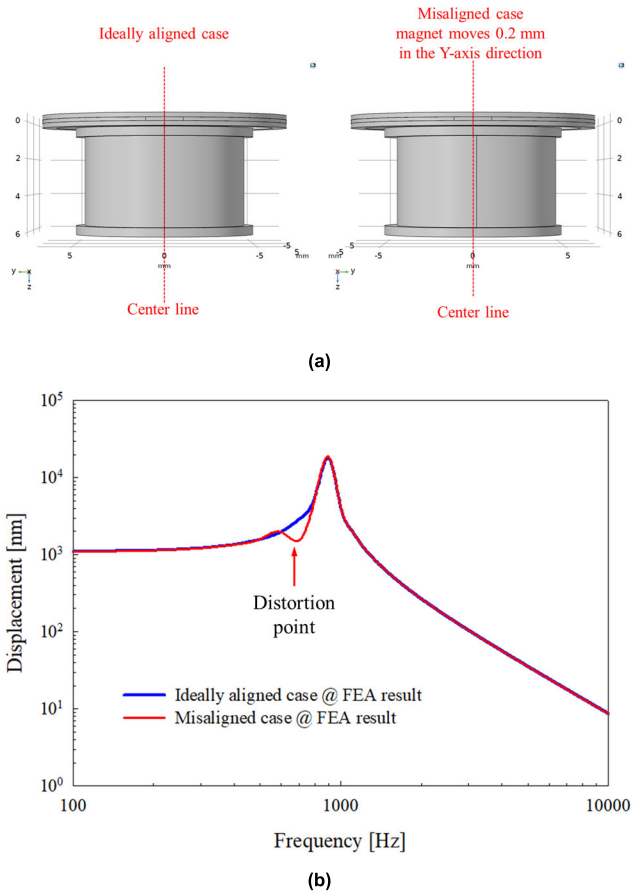

FIGURE 6. (a) Analysis model and (b) frequency characteristics according to the alignment of the vibrational membrane and magnet.

Therefore, FEA was performed at 0.5, 0.9, and 2 kHz using the 121-coordinate cantilever system derived from Fig. 4. The following procedure was performed using Matlab R2019b software to visualize the vibration magnitude of the cantilevers obtained through FEA. The vibration data derived from the 121 measurement points for each frequency were saved in a file along with the coordinates of the points. This file was read into Matlab code, and all of the measurement points were placed on a two-dimensional plane by changing only the scale of the coordinates; the relative positions of individual points were fixed. To express the magnitude of the vibration, a polygon centered on the coordinates of the point was drawn and a color corresponding to the magnitude was then applied. Specifically, for points arranged on a straight line, squares were drawn centered on the coordinates of the points, with the length of one side corresponding to the distance between points. For points arranged along a curve, arc-shaped polygons centered on each point were drawn. The polygons representing the measurement points are shown in Fig. 7, and correspond to the shape of the membrane shown in Fig. 4 rotated counterclockwise by the angle of the cantilever. Therefore, the relative positions between the measurement points in each picture are expressed identically in Figs. 4 and 7. The magnitude of the measured vibration

was normalized to within the range of 0–255. The normalized magnitude was mapped one-to-one to a color map with a gradient of 256 levels, and polygons corresponding to each point were thus assigned a color corresponding to the magnitude of their vibration. In the Matlab code, a "Jet" style color map was used. The vibrational membranes of the aligned structure in Fig. 7 had almost the same vibrational characteristics when comparing the edges (edges 1–4) of each cantilever at 0.5, 0.9, and 2 kHz. On the other hand, the vibrational membrane of the misaligned structure had different vibrational characteristics when comparing the edges of each cantilever at 0.5 and 0.9 kHz. However, the characteristics were almost the same at 2 kHz.

B. TRANSDUCER ASSEMBLY CONDITION INSPECTION

To check the assembly state of the BCI transducer manufactured in this study (Fig. 3), vibrations of the cantilevers at 0.5, 0.9, and 2 kHz were measured using LDV and a data acquisition device based on the XY coordinate system obtained through FEA. The housing of the BCI transducer was firmly fixed to the groove of the aluminum plate of the XY manual stage using cyanoacrylate, and the digital scale caliper values were set to 0. The laser (spot size 1.5 μm) generated from by the LDV was aligned perpendicular to the membrane by using a micromanipulator joystick (A-HLV-MM30; Polytec GmbH, Waldbronn, Germany). The transducer membrane is shown on the monitor screen via the built-in CCD camera of the LDV. The center point was found by drawing vertical and horizontal guidelines on the displayed membrane, and the laser spot was moved to that position. After applying a sinusoidal voltage (2.88 V_p) to the transducer, the vibration was measured while moving to the position corresponding to the 121-coordinate system using the fine adjustment handle of the XY stage. Fig. 8(a) shows the experimental environment for measuring the vibration of the BCI transducer vibrational membrane. The magnitude of the vibration of the cantilever measured at each coordinate was visualized with the same method applied previously using Matlab software. Figs. 8(b-d) shows the visualization results of the vibrational characteristics of the cantilever measured using LDV at 0.5, 0.9, and 2 kHz. The results in Figs. 8(b-d) indicate that the cantilever of the BCI transducer used in this study vibrated almost symmetrically at 0.5 kHz, 0.9, and 2 kHz. That is, the BCI transducer used in the experiment was assembled in a state in which the magnet and vibrational membrane were well aligned with the central axis.

IV. DISCUSSION

To compare the vibration magnitude of the four cantilevers constituting the vibrational membrane more clearly, the standard deviation was calculated based on the displacement of each cantilever edge using the following equations.

$$X = \frac{1}{n}(x_1 + x_2 + x_3 + \cdots + x_n) \tag{1}$$

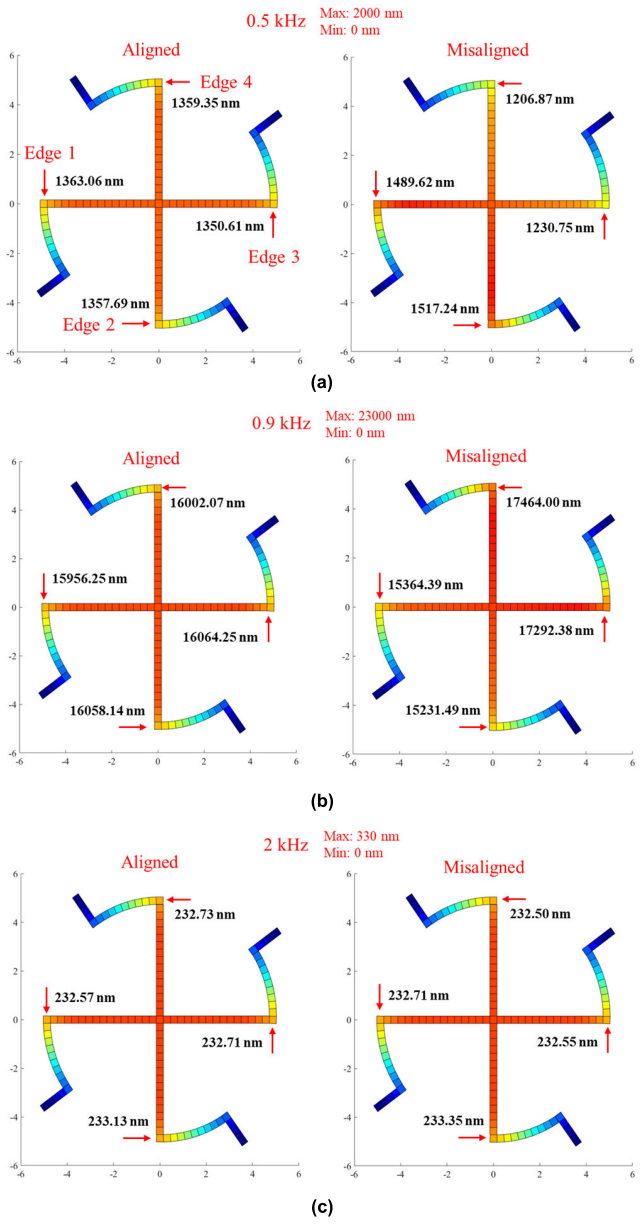

FIGURE 7. Comparison of the vibration magnitude of the vibrational membrane between aligned and misaligned cases: (a) 0.5 kHz, (b) 0.9 kHz, and (c) 2 kHz.

$$S^2 = \frac{(x_1 - X)^2 + (x_2 - X)^2 + \cdots + (x_n - X)^2}{n} \tag{2}$$

$$S = \sqrt{S^2} \tag{3}$$

Here, X is the average of the edges, n is the number of edges, x is the value for each edge, S^2 is the variance of the edges, and S is the standard deviation of the edges.

The standard deviation of the displacement was used to quantify the magnitude of the vibration generated at each edge (edges 1–4) of the cantilever. A large standard deviation indicates that the magnitude of vibration of each edge is different, while a small standard deviation indicates that the magnitude of vibration is similar at each edge.

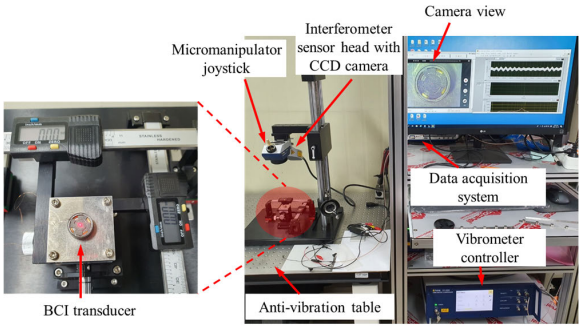

(a)

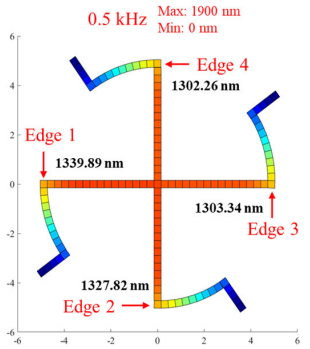

(b)

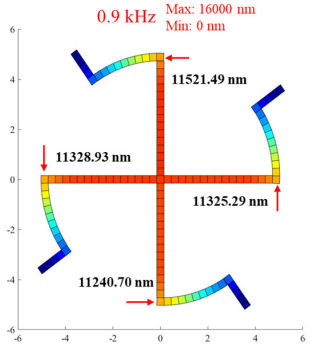

(c)

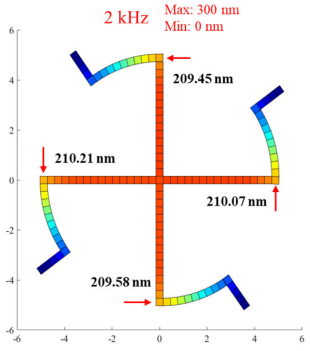

(d)

FIGURE 8. Vibration measurement of the manufactured BCI transducer. (a) Experimental environment. (b) Vibrational characteristics at 0.5 kHz. (c) Vibrational characteristics at 0.9 kHz. (d) Vibrational characteristics at 2 kHz.

TABLE 1. Displacement at the edge (aligned case, FEA).

Freq. (kHz)	Edge 1 (nm)	Edge 2 (nm)	Edge 3 (nm)	Edge 4 (nm)	Mean (nm)	Standard deviation (nm)
0.5	1363.06	1357.69	1350.61	1359.35	1357.68	4.52
0.9	15956.25	16058.14	16064.25	16002.07	16020.18	44.15
2	232.57	233.13	232.71	232.73	232.79	0.21

TABLE 2. Displacement at the edge (misaligned case, FEA).

Freq. (kHz)	Edge 1 (nm)	Edge 2 (nm)	Edge 3 (nm)	Edge 4 (nm)	Mean (nm)	Standard deviation (nm)
0.5	1489.62	1517.24	1230.75	1206.87	1361.12	142.89
0.9	15364.39	15231.49	17292.38	17464.00	16338.07	1042.95
2	232.71	233.35	232.55	232.50	232.78	0.34

TABLE 3. Displacement at the edge (measurement results).

Freq. (kHz)	Edge 1 (nm)	Edge 2 (nm)	Edge 3 (nm)	Edge 4 (nm)	Mean (nm)	Standard deviation (nm)
0.5	1339.89	1327.82	1303.34	1302.26	1318.33	16.11
0.9	11328.93	11240.70	11325.29	11521.49	11354.10	102.89
2	210.21	209.58	210.07	209.45	209.83	0.32

Tables 1 and 2 show values obtained by FEA for alignment and misalignment cases (from Fig. 7), and Table 3 shows values measured from the BCI transducer (Fig. 8). The highest standard deviation was observed at 0.9 kHz, where resonance occurred. Comparison of the FEA results in Tables 1 and 2 indicates that the standard deviation value of misaligned cases was more than 20 times higher than for aligned cases at 0.5 and 0.9 kHz. However, there was no marked difference at 2 kHz. Table 3, which shows the measurement results of the manufactured BCI transducer, indicates higher standard deviation values at 0.5 and 0.9 kHz than in the ideal aligned case (Table 1), but the values were eight times lower than in the misaligned case (Table 2). Similarly, there was no significant difference at 2 kHz. In summary, misalignment was reflected in a high standard deviation value in a low frequency band (below 1 kHz) and a high vibration magnitude. Therefore, distortion characteristics appeared in the low frequency band, as indicated by the red solid line in Fig. 6.

Finally, to check whether the system implemented can identify a misaligned BCI transducer, we assembled one in the same manner as the misaligned FE model (Fig. 6) and tested it as follows. A misaligned transducer was assembled so that the magnet deviated 0.2 mm from the central axis using an aluminum jig to align the centers of the magnet and metal plate. The rest of the assembly process and vibrational

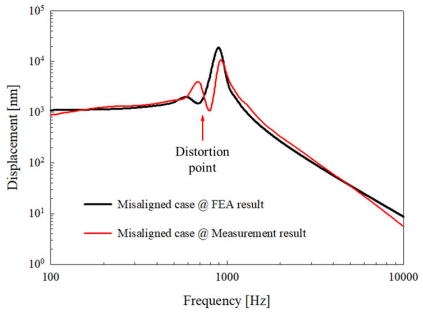

(a)

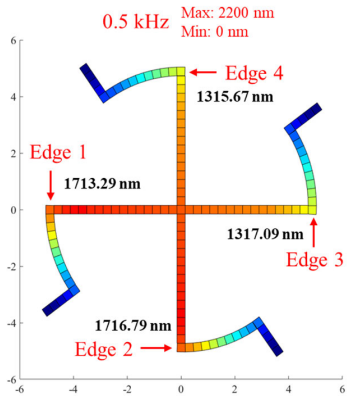

(b)

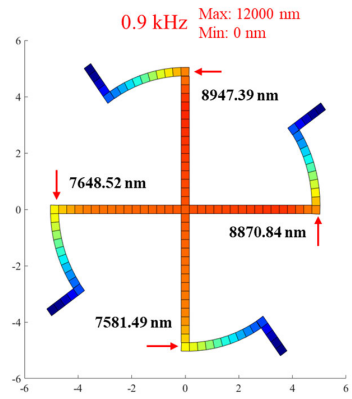

(c)

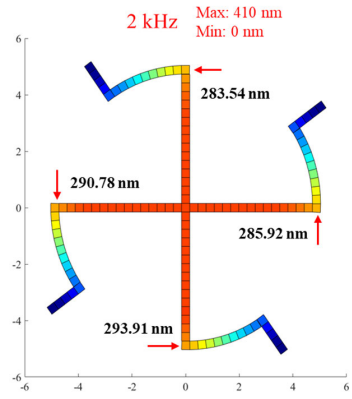

(d)

FIGURE 9. Measuring the vibration of a misaligned BCI transducer. (a) Frequency response characteristics. (b) Vibrational characteristics at 0.5 kHz. (c) Vibrational characteristics at 0.9 kHz. (d) Vibrational characteristics at 2 kHz.

TABLE 4. Displacement at the edge (misaligned BCI transducer).

Freq. (kHz)	Edge 1 (nm)	Edge 2 (nm)	Edge 3 (nm)	Edge 4 (nm)	Mean (nm)	Standard deviation (nm)
0.5	1713.29	1716.79	1317.09	1315.67	1515.71	199.33
0.9	7648.52	7581.49	8870.84	8947.39	8262.06	648.05
2	290.78	293.91	285.92	283.54	288.54	4.05

membrane measurements were the same as in the original method. Fig. 9(a) shows the frequency response characteristics of the misaligned BCI transducer (red solid line), which showed distortion characteristics at a specific frequency band similar to the frequency response characteristics of the misaligned FE model (black solid line). Figs. 9(b-d) show the visualization results of the vibration of the misaligned BCI transducer cantilever measured using LDV at 0.5, 0.9, and 2 kHz. When the edges of each cantilever were compared at 0.5 and 0.9 kHz, the vibrational membrane of the misaligned BCI transducer showed different vibration characteristics. At 2 kHz, however, it had almost the same vibration characteristics. The standard deviation was calculated for the displacement of each edge using equations (1) – (3). Table 4 shows the displacements measured at edges 1–4 of the misaligned BCI transducer. The misaligned BCI transducer had a standard deviation 6- to 12-times higher than those of aligned BCI transducers (Table 3). These experimental results show that our system can identify the alignment and misalignment of the BCI transducer.

V. CONCLUSION

In this study, a two-axis measurement system based on an LDV and XY manual stage was used to inspect the assembly condition of a BCI transducer. To obtain the four cantilever coordinates constituting the vibrational membrane, two digital scale calipers were combined with the X and Y axes of the stage. In addition, FEA was used to obtain the position coordinate system of each cantilever. After designing a BCI transducer, FEA analysis was performed for the cases of alignment and misalignment of the vibrational membrane and permanent magnet. After visualizing the motion of the cantilever using Matlab software, the vibration magnitudes of the alignment and misalignment cases were compared (0.5, 0.9, and 2 kHz). When the vibrational membrane and magnet were ideally aligned, the four cantilevers at 0.5, 0.9, and 2 kHz had almost the same vibration magnitude. On the other hand, in the case of misalignment, the four cantilevers had different magnitudes of vibration at 0.5 and 0.9 kHz. However, the vibration magnitudes were almost the same at 2 kHz. Based on the FEA results, the assembly condition of the BCI transducer manufactured for this study was analyzed using a two-axis measurement system and a single-point LDV. According to the coordinate system obtained from the

FEA model, the vibration magnitude of the cantilever was measured at 0.5, 0.9, and 2 kHz, and then visualized using the same method. The results indicated that the four cantilevers of the manufactured transducer had almost the same vibration magnitude.

To numerically compare the vibration magnitudes of the four cantilevers, the standard deviation was calculated from the displacement of each edge. The fabricated BCI transducer had a higher (3.5 times at 0.5 kHz and 2.3 times at 0.9 kHz) standard deviation than the ideally aligned FEA model, but it was about 8 times lower (at 0.5 and 0.9 kHz) than that of the misaligned case. The results of numerical comparison indicated that although the vibrational membrane and magnet were not completely aligned with the central axis of the manufactured BCI transducer, the transducer was very well assembled.

Finally, a verification experiment was performed to confirm that the implemented system can identify the alignment state of a misaligned BCI transducer. After assembling the magnet so that it deviates from the central axis, the frequency response characteristics and vibration characteristics at each point of the cantilever were measured, along with the standard deviation. Unaligned BCI transducers had a higher standard deviation (at least 6 times) than the aligned BCI transducers. These results confirm that the measurement system implemented here can be used to inspect the alignment of the vibrational membrane and magnet, which may cause distortion before the BCI transducer is completely assembled.

REFERENCES

[1] R. L. Goode, M. L. Rosenbaum, and A. J. Maniglia, "The history and development of the implantable hearing AID," *Otolaryngol. Clinics North Amer.*, vol. 28, no. 1, pp. 1–16, Feb. 1995.

[2] D. S. Haynes, J. A. Young, G. B. Wanna, and M. E. Glasscock, "Middle ear of implantable hearing devices: An overview," *Trends Amplification*, vol. 13, no. 3, pp. 206–214, Sep. 2009.

[3] L. Lassaletta, I. Sánchez-Cuadrado, J. M. Espinosa, Á. Batuecas, C. Cenjor, M. J. Lavilla, L. Cavallé, A. Huarte, F. Nuñez, M. Manrique, Á. Ramos, C. de Paula, and E. Gil-Carcedo, "Active middle ear implants," *Acta Otorrinolaringol.*, vol. 70, no. 2, pp. 112–118, Mar. 2019.

[4] M. Tisch, "Implantable hearing devices," *GMS Current Topics Otorhinolaryngol.-Head Neck Surg.*, vol. 16, pp. 1–22, Dec. 2019.

[5] R. M. Rhodes and B. S. T. Do, "Future of implantable auditory devices," *Otolaryngol. Clinics North Amer.*, vol. 52, no. 2, pp. 363–378, Apr. 2019.

[6] D. Calero, S. Paul, A. Gesing, F. Alves, and J. A. Cordioli, "A technical review and evaluation of implantable sensors for hearing devices," *Biomed. Eng. OnLine*, vol. 17, no. 1, pp. 1–26, Feb. 2018.

[7] D. H. Shin and J.-H. Cho, "Design and development of a tri-coil bellows transducer for RW-drive implantable middle-ear hearing aid using FEA," *IEEE/ASME Trans. Mechatronics*, vol. 23, no. 3, pp. 1436–1444, Jun. 2018.

[8] A. Mudry and L. Dodelé, "History of the technological development of air conduction hearing aids," *J. Laryngol. Otol.*, vol. 114, no. 6, pp. 418–423, Jun. 2000.

[9] H. H. Kim and D. M. Barrs, "Hearing aids: A review of what's new," *J. Otolaryngol.-Head Neck Surg.*, vol. 134, no. 6, pp. 1043–1050, Jun. 2006.

[10] E. E. Johnson, "Prescriptive amplification recommendations for hearing losses with a conductive component and their impact on the required maximum power output: An update with accompanying clinical explanation," *J. Amer. Acad. Audiol.*, vol. 24, no. 6, pp. 452–460, Jun. 2013.

[11] D. H. Shin, K. W. Seong, S. Puria, K.-Y. Lee, and J.-H. Cho, "A tri-coil bellows-type round window transducer with improved frequency characteristics for middle-ear implants," *Hearing Res.*, vol. 341, pp. 144–154, Nov. 2016.

[12] A. L. Gesing, Z. N. Masson, D. C. Arellano, F. Alves, S. Paul, and J. A. Cordioli, "Middle ear ossicular chain vibration detection by means of an optimized MEMS piezoelectric accelerometer," *IEEE Sensors J.*, vol. 19, no. 6, pp. 2079–2086, Mar. 2019.

[13] D. H. Shin, K. W. Seong, H. H. Nakajima, S. Puria, and J.-H. Cho, "A piezoelectric bellows round-window driver (PBRD) for middle-ear implants," *IEEE Access*, vol. 8, pp. 137947–137954, Jul. 2020.

[14] S. Busch, T. Lenarz, and H. Maier, "Comparison of alternative coupling methods of the vibrant soundbridge floating mass transducer," *Audiol. Neurotol.*, vol. 21, no. 6, pp. 347–355, Jan. 2017.

[15] A. Müller, P. Mir-Salim, N. Zellhuber, R. Helbig, M. Bloching, T. Schmidt, S. Koscielny, O. C. Dziemba, S. K. Plontke, and T. Rahne, "Influence of floating-mass transducer coupling efficiency for active middle-ear implants on speech recognition," *Otol. Neurotol.*, vol. 38, no. 6, pp. 809–814, Jul. 2017.

[16] T. M. Eßinger, M. Koch, M. Bornitz, N. Lasurashvili, M. Neudert, and T. Zahnert, "Sensor-actuator component for a floating mass transducer-based fully implantable hearing aid," *Hearing Res.*, vol. 378, pp. 157–165, Jul. 2019.

[17] I. Mosnier *et al.*, "Benefit of the vibrant soundbridge device in patients implanted for 5 to 8 years," *Ear Hearing*, vol. 29, no. 2, pp. 281–284, Apr. 2008.

[18] J. M. Lee, J. Jung, I. S. Moon, S. H. Kim, and J. Y. Choi, "Benefits of active middle ear implants in mixed hearing loss: Stapes versus round window," *Laryngoscope*, vol. 127, no. 6, pp. 1435–1441, Jun. 2017.

[19] U. A. Gamm, M. Grossöhmichen, R. B. Salcher, N. K. Prenzler, T. Lenarz, and H. Maier, "Optimum coupling of an active middle ear actuator: Effect of loading forces on actuator output and conductive losses," *Otol. Neurotol.*, vol. 40, no. 6, pp. 789–796, Jul. 2019.

[20] J. Wales, K. Gladiné, P. Van de Heyning, V. Topsakal, M. von Unge, and J. Dirckx, "Minimally invasive laser vibrometry (MIVIB) with a floating mass transducer—A new method for objective evaluation of the middle ear demonstrated on stapes fixation," *Hearing Res.*, vol. 357, pp. 46–53, Jan. 2018.

[21] B. Håkansson, S. Reinfeldt, M. Eeg-Olofsson, P. Östli, H. Taghavi, J. Adler, J. Gabrielsson, S. Stenfelt, and G. Granström, "A novel bone conduction implant (BCI): Engineering aspects and pre-clinical studies," *Int. J. Audiol.*, vol. 49, no. 3, pp. 203–215, Jan. 2010.

[22] R. Weiss, A. Loth, M. Leinung, S. Balster, D. Hirth, T. Stöver, S. Helbig, and S. Kramer, "A new adhesive bone conduction hearing system as a treatment option for transient hearing loss after middle ear surgery," *Eur. Arch. Oto-Rhino-Laryngol.*, vol. 277, no. 3, pp. 751–759, Mar. 2020.

[23] A. Canale, V. Boggio, A. Albera, M. Ravera, F. Caranzano, M. Lacilla, and R. Albera, "A new bone conduction hearing aid to predict hearing outcome with an active implanted device," *Eur. Arch. Oto-Rhino-Laryngol.*, vol. 276, no. 8, pp. 2165–2170, Aug. 2019.

[24] A. Magele, P. Schoerg, B. Stanek, B. Gradl, and G. M. Sprinzl, "Active transcutaneous bone conduction hearing implants: Systematic review and meta-analysis," *PLoS ONE*, vol. 14, no. 9, Sep. 2019, Art. no. e0221484.

[25] L. Placke, E. Appelbaum, A. Patel, and A. Sweeney, "Bone conduction implants for hearing rehabilitation in skull base tumor patients," *J. Neurol. Surg. B, Skull Base*, vol. 80, no. 2, pp. 139–148, Apr. 2019.

[26] J. P. Richards, J. T. Symms, K. Beasley, and H. M. S. Coffman, "Bone conduction implants," *Current Opinion Otolaryngol. Head Neck Surg.*, vol. 28, no. 5, pp. 308–313, Oct. 2020.

[27] A. Sarasty and M. Zernotti, "Active bone conduction prosthesis: BoneBridgeTM," *Int. Arch. Otorhinolaryngol.*, vol. 19, no. 4, pp. 343–348, Oct. 2015.

[28] M. Manrique, I. Sanhueza, R. Manrique, and J. de Abajo, "A new bone conduction implant: Surgical technique and results," *Otol. Neurotol.*, vol. 35, no. 2, pp. 216–220, Feb. 2014.

[29] S. Reinfeldt, B. Håkansson, H. Taghavi, and M. Eeg-Olofsson, "New developments in bone-conduction hearing implants: A review," *Med. Devices, Evidence Res.*, vol. 8, pp. 79–93, Jan. 2015.

[30] D. H. Shin, K. W. Seong, E. S. Jung, J.-H. Cho, and K.-Y. Lee, "Design of a dual-coil type electromagnetic actuator for implantable bone conduction hearing devices," *Technol. Health Care*, vol. 27, pp. 445–454, Jun. 2019.
[31] S. H. Lee, K. W. Seong, K.-Y. Lee, and D. H. Shin, "Optimization and performance evaluation of a transducer for bone conduction implants," *IEEE Access*, vol. 8, pp. 100448–100457, May 2020.
[32] H. Taghavi, B. Håkansson, and S. Reinfeldt, "A novel bone conduction implant system: Analog radio frequency data and power link design," in *Proc. 9th IASTED Int. Conf. Biomed. Eng.*, Innsbruck, Austria, 2012, pp. 327–335.

DONG HO SHIN received the B.S. degree in electronics engineering from Dongseo University, Busan, South Korea, in 2009, and the M.S. and Ph.D. degrees from the School of Electronics Engineering, Kyungpook National University, South Korea, in 2011 and 2016, respectively.

From 2016 to 2019, he was a Research Fellow at the Institute of Biomedical Engineering Research, Kyungpook National University, where he is currently working as a Research Professor. His research interests include electronic and mechanical system of medical instruments and middle-ear implants transducer.

HUI-SUP CHO received the B.S. and M.S. degrees in electronics engineering and the Ph.D. degree in biomedical engineering from Kyungpook National University, Daegu, South Korea, in 1999, 2001, and 2017, respectively.

From 2001 to 2005, he was a Senior Researcher at LG Electronics, South Korea. He currently works as a Senior Researcher at Daegu Gyeongbuk Institute of Science and Technology, South Korea. His research interests include electronic and mechanical system of medical instruments and radar technology applications for human body.